Talanta 182 (2018) 348–353

Contents lists available at ScienceDirect

Talanta

journal homepage: www.elsevier.com/locate/talanta

Core-shell assay based aptasensor for sensitive and selective thrombin detection using dark-field microscopy

Rui Yang[a], Shuwen Liu[c,d], Zhenjie Wu[a,b], Ying Tan[c,d,*], Shuqing Sun[a,b,*]

[a] Institute of Optical Imaging and Sensing, Shenzhen Key Laboratory for Minimal Invasive Medical Technologies, Graduate School at Shenzhen, Tsinghua University, Shenzhen 518055, People's Republic of China
[b] Department of Physics, Tsinghua University, Beijing 100084, People's Republic of China
[c] Department of Chemistry, Tsinghua University, Beijing 100084, People's Republic of China
[d] State Key Laboratory of Chemical Oncogenomics, The Graduate School at Shenzhen, Tsinghua University, Shenzhen 518055, People's Republic of China

ARTICLE INFO

Keywords:
AuNPs
DFM
Aptasensor
Thrombin

ABSTRACT

In this work, we developed a robust and ultrasensitive bio-sensor based on the target-aptamer recognition strategy and microscopic enumeration of gold nanoparticles (AuNPs) using dark field microscopy (DFM). The aptasensor with a core-shell structure consisting of a magnetic bead (MB), aptamer and AuNPs was fabricated by complementary hybridization of the DNA probe on the AuNPs surface to the aptamer coupled to the MB. Upon addition of the target molecule, the strong interaction between the aptamer and the target molecule, thrombin, results in the release of the AuNPs from the MB. The quantities of thrombin is therefore linearly correlated to the number of the released AuNPs, which can be digitally counted using DFM. To demonstrate the feasible use of the aptasensor for target detection, thrombin was evaluated as the model target. The limit of detection was determined to be 2.54 fM with dynamic range of 6 fM–100 fM. When the concentration of thrombin exceeded 100 fM, the counted number of AuNPs didn't correlate linearly to molecules of thrombin anymore, as the nanoparticles aggregated partly due to high concentration. However, the color of the solution changes to purple and the concentration of free AuNPs can be conveniently quantified by UV–Vis spectroscopy for up to 100 nM. It is noteworthy that our aptasensor is very easy to operate and requires neither complex isolation and amplification processes nor expensive instruments and consumables. Furthermore, this strategy can be easily generalized to other targets by replacing the corresponding aptamers and show great potential for the detection of biomarkers in clinical samples.

1. Introduction

The development of biosensors that recognize biological targets or processes has attracted increasing attention. Proteins, large biomolecules or macromolecules, perform various functions in organisms, including accelerating metabolic reactions, responding to stimuli, replicating DNA, and transporting molecules. The significant changes in proteins can reveal the physiological and pathological processes of an organism, which are regarded as biomarkers, indicating the biological state of a disease. These proteins are of great significance in basic research of life science [1,2], disease diagnosis [3–5], drug research [6,7], human health analysis [8,9] and biological safety monitoring [10,11]. Protein recognition based on the specificity of antigen and antibody of immune response is a widely used technique [12–14]. However, some drawbacks such as the time-consuming, costly and difficult in chemical modification and immunogenic preparation of antibody produced by the organism, restrict the use of protein analysis. Therefore, investigations aimed at the development of more convenient and efficient protein recognition are highly significant in biological systems.

Aptamers generated by the Systematic Evolution of Ligands by Exponential enrichment (SELEX) technique [15–19], are sequences of oligonucleotides that can specifically bind to a target with a stable structure, such as G-quadruplex [20], hairpin [21], and pseudoknot [22]. In contrast to antibodies, aptamers can be easily synthesized and chemically modified with little immunogenicity. The target molecules of aptamer are widely distributed, including metal ions, organic small molecules, proteins, viruses, cells and others, which allowed a range of applications of aptamer for sensitive detection of different species. Aptamers have been considered an excellent molecular recognition element due to their high affinity and good specificity for the target through complementary pairing, complementary shape, van der Waals forces, electrostatic interaction and hydrogen bonds.

* Correspondence to: Graduate School at Shenzhen, Tsinghua University, Shenzhen 518055, People's Republic of China.
E-mail addresses: tan.ying@sz.tsinghua.edu.cn (Y. Tan), sun.shuqing@sz.tsinghua.edu.cn (S. Sun).

https://doi.org/10.1016/j.talanta.2018.01.070
Received 31 October 2017; Received in revised form 12 January 2018; Accepted 29 January 2018
Available online 31 January 2018
0039-9140/

Gold nanoparticles (AuNPs) have been extensively studied for biological applications due to their inherent characteristics such as easy surface modification and good biocompatibility. Gold nanoparticle and aptamer composites have no significant systemic toxicity was observed in rats (1 mg/kg of body weight) [23]. AuNPs can be facilely prepared with well-defined shapes and sizes under controllable conditions that directly affect the optical properties of AuNPs [24] and can be utilized in a variety of fields. Several methods have been developed to assay target-aptamer recognition using AuNPs, including colorimetry [25,26], fluorescence [27,28], chemiluminescence [29], electrochemistry [30], surface-enhanced Raman [31] and others. However, the sensitivity based on the measurement of the collective signals of large number of nanoparticles is generally limited, which lead to the detection of limits achieved in the range of nanomolar to picomolar in concentration. Actually, owning to the excellent optical properties of AuNPs, especially the localized surface plasmon resonance (LSPR) effect, each particle can be detected digitally with excellent signal to noise ratio. Using a DFM, AuNPs can be unambiguously identified and quantified [32,33] which provides an excellent methodology for ultrasensitive detection for target molecules. Herein, we developed a simple and cost-effective aptasensor, which combined 1 to 1 substitution of target molecule for AuNPs through aptamer-target interaction and subsequent spectroscopic quantification/microscopic identification and enumeration of replaced AuNPs, with a detection limit as low as the fM level and an extremely wide dynamic range. The strategy is depicted schematically in Scheme 1. First, biotin-conjugated aptamers are immobilized on the surface of the streptavidin-conjugated magnetic beads (MBs) through a biotin-streptavidin interaction. AuNPs modified with DNA probes with a sequence complementary to the aptamer were added in excess of the aptamer [34,35]. An aptasensor with the core-shell structure of MB/aptamers/AuNPs has thus been fabricated. In the presence of a target, the aptamer recognizes and forms a secondary structure with the target, interrupting the complementary pairing and leading to the release of AuNPs from the MBs. The dissociated AuNPs are then quantified by ultraviolet spectroscopy or DFM digitally due to their excellent optical properties. As proof of concept, thrombin as a serine protease, playing an important role in molecular biology, is used as the model target in the present work.

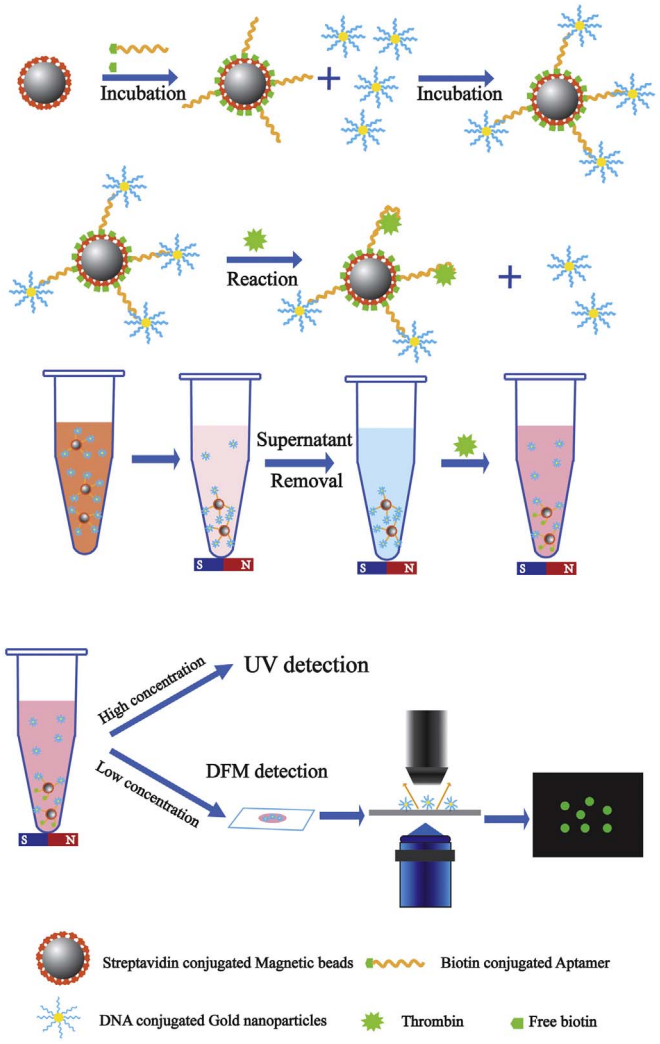

Scheme 1. Schematic illustration for detection of the target. Thrombin is used as the model target.

2. Materials and methods

2.1. Reagents

DNA sequences were synthesized by Sangon Biotechnology Co. Ltd. (Shanghai, China). The aptamer sequence was 5′-biotin- TTTTTTTTTT TTTTTTTTTTGGTTGGTGTGGTTGG-3′. The complementary sequence (cDNA) was 5′-SH-TTTTTTTTTTTTTTTTTTTTTCCAAC-3′. Tris (2-carboxyethyl) phosphine (TCEP), hydrogen tetrachloroaurate (III) hydrate ($HAuCl_4{\cdot}3H_2O$), thrombin (Thr), Cytochrome (Cyt), lysozyme (Lys), IgG from rabbit serum, bovine serum albumin (BSA), and Trypsin (Try) were obtained from Sigma-Aldrich (USA). Dynabeads M-280 Streptavidin was purchased from Thermo Fisher. (3-Aminopropyl) triethoxysilane (APTES) was purchased from Nanjing Chen Gong Co., Ltd. The water used in the experiment was ultrapure water from the Millipore water purification system.

2.2. Instrumentation

Scanning electron microscope (SEM) images were obtained using a ZEISS SUPRA®55 instrument (Carl Zeiss, Germany). Size measurement and distributions were measured by dynamic light scattering (DLS) on a Malvern Zetasizer Nano-ZS90 system (Malvern, Britain). Absorbance measurements were performed using a microplate reader (Tecan infinite M1000 Pro reader, Switzerland). Dark-field microscopic images were recorded using an optical BX53 microscope equipped with a color CCD (Olympus, Japan).

2.3. Synthesis of different sizes of AuNPs

The seed of the gold granule was produced by the sodium citrate reduction method. Then, using hydroxylamine hydrochloride to reduce the chloroauric acid with the addition of obtained gold granule as seeds, the gold particles with different particle sizes were produced. The detailed procedure was as follows [36]: 99 mL of ultrapure water was added to 1 mL of $HAuCl_4$ solution (24 mM), and 10 mL of sodium citrate (14.55 mM) was subsequently added. The mixture was heated under 110 ℃ for 20 min, followed by cooling in ice water for 10 min. The dark red reactive liquid was filtered through a 0.22 μm filter. The liquid was subjected to density gradient centrifugation, carried out by centrifuging at 8600 rpm for 10 min, resulting in the removal of the supernatant after centrifuging at 4000 rpm for another 10 min. The light pink supernatant was used as the seed solution. Next, different sizes of gold particles were prepared by adding 1 mL of 40 mM hydroxylamine hydrochloride solution and 1 mL of $HAuCl_4$ solution (3.52 mM) into the 1–6 mL seed solution samples. The 10 mL of gold solution was condensed to 1 mL by centrifugal washing.

2.4. Functional modification of gold nanoparticles

After incubating TCEP with cDNA for 1 h, the obtained gold particles were mixed with cDNA solution with the molar concentration ratio of cDNA: AuNPs = 10000:1 and incubated overnight. Then, the salt

solution (0.3 M NaCl, 4 mM $MgCl_2$, 0.3% SDS, pH = 8.0) was added ten times with shaking evenly and ultrasonic treatment for 10–15 s each time to reach the final volume ratio of 1:1. The solution was then aged for 16 h. Excess cDNA was removed by centrifugation at 4500 rpm for 5 min, and the red precipitate was washed three times with 10 mM PB solution (0.01% SDS, pH = 7.4).

2.5. Aptasensor fabrication

The MBs modified with streptavidin were suspended in a B&W buffer (10 mM pH 7.5 Tris-HCl, 1 mM EDTA, 2 M NaCl), followed by the addition of a biotinylated aptamer (0.1 μM, 15 min) and free biotin (100 μM, 15 min) incubated in turn at room temperature. Then, the mixture was subjected to washing and magnetic separation to remove the free aptamer. The formation of the core-shell structure aptasensor was achieved by adding cDNA-modified AuNPs to the dispersion of aptamer-functionalized MBs in a hybridization buffer (10 mM PBS, pH 7.4, 0.3 mM NaCl, 0.01% SDS) for 30 min, as described above. Following the magnetic separation, the color of the solution changed from red to light purple, indicating that a significant amount of AuNPs had been immobilized to MBs through DNA hybridization. The as-prepared aptasensor was washed and stored in a refrigerator.

2.6. Modification of the glass slide

The glass slide was first soaked in a piranha solution (concentrated sulfuric acid: hydrogen peroxide = 7:3) for 6 h to remove any contaminants. After rinsing with a large amount of pure water, it was soaked in 10% (v/v) APTES ethanol solution for 6 h and then rinsed with pure water and dried in a vacuum drying oven.

2.7. Detection of thrombin

The detection of thrombin was conducted by adding different concentrations of thrombin to the as-prepared aptasensor in a solution consisting of 20 mM Tris-HCl, pH 7.4, 140 mM NaCl, 1 mM $MgCl_2$, 5 mM KCl, 1 mM $CaCl_2$ and 1 mg/mL BSA (reaction liquid) for 30 min. After magnetic separation, the supernatant was collected and the quantification of AuNPs released from the aptasensor was performed either using UV–Vis spectroscopy or DFM for high or low concentrations of thrombin, respectively, depending on whether the supernatant showed any color. For higher concentration the red color is easily observed and UV–Vis spectrometer is used to quantify the AuNPs. On the other hands, when the concentration is low, it is colorless and DFM method is used in detection.

For ultraviolet measurements, 50 μL of supernatant obtained from the reaction liquid was added to a 96-well plate, and the absorbance at 530 nm was recorded. For the DFM imaging, 5 μL of supernatant was dropped on the modified glass slides and covered with a cover slide. The images were taken in the dark field microscope and imported into the MATLAB software to quantify the number of AuNPs. A linear relationship between the thrombin concentrations and the counts of AuNPs was obtained.

3. Results and discussion

3.1. Modification and characterization of AuNPs

The optical properties of AuNPs are affected by their shape and size. To optimize the size of AuNPs for dark-field microscopic counting, 6 kinds of AuNPs with sizes ranging from 47 to 80 nm were synthesized and characterized by UV, SEM, Malvern Zetasizer Nano-ZS90 and DFM. As shown in Fig. 1A, the AuNPs exhibited a strong absorption that redshifted with the increase of AuNP sizes. The particle sizes were calculated to be 80 nm, 73 nm, 70 nm, 63 nm, 48 nm, and 47 nm using a Malvern Zetasizer Nano-ZS90 instrument. Based on electron microscopy, all AuNPs showed uniform sizes and regular shapes. (Fig. 1B a-f)

Fig. 1B shows the DFM images of AuNPs with different sizes. It is

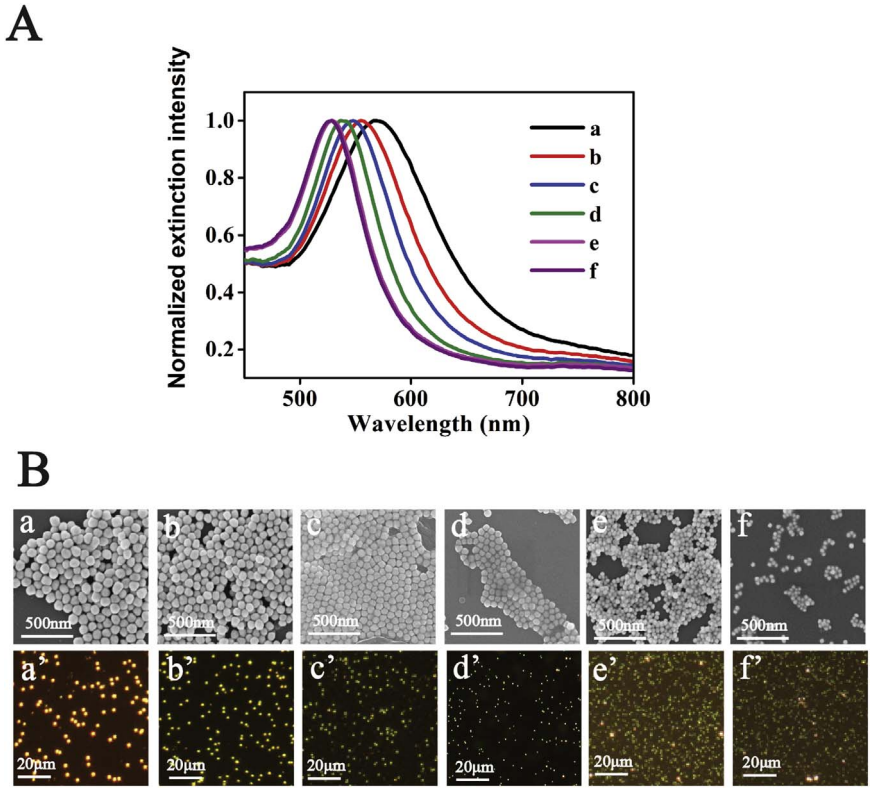

Fig. 1. Characteristics of AuNPs. (A) UV–Vis spectroscopy of six sizes of AuNPs. (B) a-f: SEM images of the six AuNPs, the particle sizes were calculated to be (a) 80 nm, (b) 73 nm, (c) 70 nm, (d) 63 nm, (e) 48 nm, and (f) 47 nm. a′-f′: Dark filed microscope images of the six AuNPs, (a′): 80 nm, (b′): 73 nm, (c′): 70 nm, (d′): 63 nm, (e′): 48 nm, and (f′): 47 nm.

clear that the larger AuNPs scatter bright yellow light, while the smaller ones scatter green light. The different AuNPs can be used in this system. In this paper, 63 nm particles is taken as an example to be used in the following studies.

3.2. Aptasensor synthesis and characterization

MBs modified with aptamers through biotin-streptavidin interaction and AuNPs modified with complementary DNA through gold thiol bonding were used to fabricate core-shell structured aptasensors through DNA complementary pairing. Fig. 2a and b show the images of aptamer-modified MBs and AuNPs coupled MBs, respectively. It can be clearly seen that AuNPs were attached to MBs demonstrating the core-shell structure of the aptasensor was constructed successfully. Fig. 2c shows the color of the aptasensor solution turned into red after the addition of thrombin in a buffer solution for 30 min, while it remains colorless after the addition of buffer without thrombin (Fig. 2d). It is evident that after adding the target, the aptamer formed the G-quadruplex structure that destroyed the base pairing interaction between the aptamer and cDNA, resulting in the dissociation of AuNPs from MBs. After magnetic separation, the amount of free AuNPs associated with the concentration of target molecules in the supernatant liquid was quantified by either UV measurement or DFM.

3.3. Recognition of thrombin

Sensitivity and stability are very significant for a detection system. To obtain a sensitive and stable signal, we optimized the recognition time of thrombin. Fig. S1 reveals that the absorbance of the supernatant containing free AuNPs at 530 nm increased significantly with the increase of the incubation time of thrombin and reached a plateau at approximately 30 min, indicating that the reaction between aptamer and thrombin has been completed. Thus, 30 min was taken as the optimal incubation time of thrombin in the subsequent experiments.

Due to the strong optical absorption and scattering characteristic of AuNPs, the detection of thrombin could be performed conveniently and sensitively by the UV–Vis spectroscopy and DFM. The high concentrations of thrombin led the sufficient number of free AuNPs to dissociate from MBs, which could be observed by the UV–Vis spectroscopy due to the strong optical extinction of AuNPs at 530 nm. Fig. 2e shows that a good linear correlation was present between the absorbance and thrombin concentrations in the 0.5–100 nM range, suggesting that the high concentration of thrombin could be detected by this biosensor. The limit of detection (LOD) was calculated to be 290 pM using the equation LOD = 3 × Sb/S.

For the very low concentrations of thrombin, the weak signal caused by the few free AuNPs, which cannot be monitored by UV–Vis spectroscopy, was detected sensitively by DFM due to the LSPR of AuNPs. To reduce background interference, an ND25 light filter was used in the recording process. The transmittance of the filter is 25%, which can adjust the light intensity of the light source and reduce the light of the

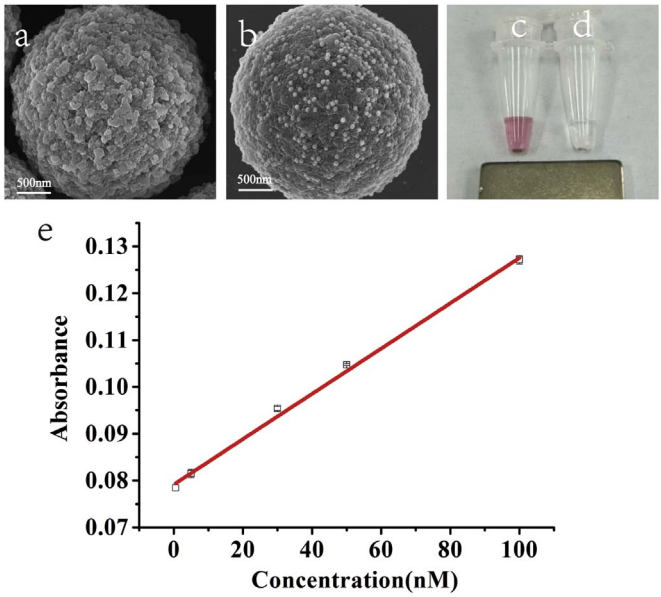

Fig. 2. (a) SEM image of an unmodified magnetic bead; (b) SEM image of core-shell structure of an aptasensor; (c) Reaction solution after adding the thrombin; (d) The control solution without the thrombin; (e) Linear relationship between absorbance and thrombin concentrations. The error bar was the standard deviation value of three repetitions.

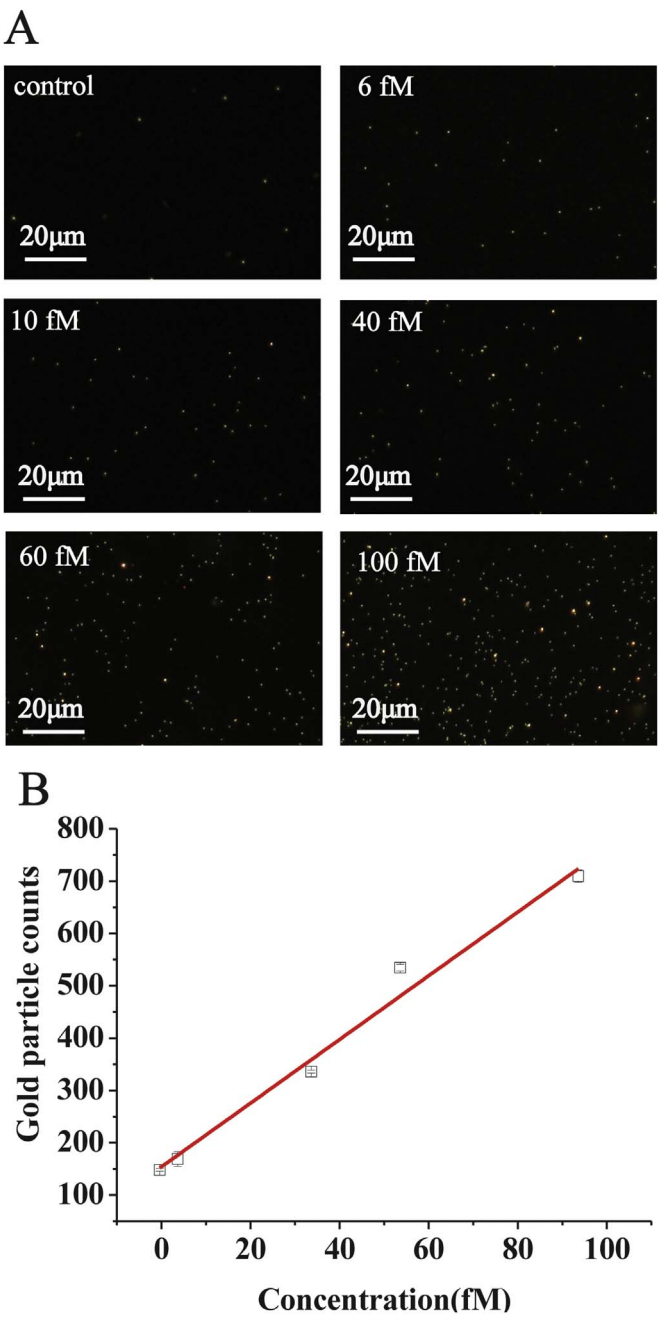

Fig. 3. Thrombin detection by DFM. A) DFM images of AuNPs: control, 6 fM, 10 fM, 40 fM, 60 fM and 100 fM. Images were recorded using a 150 W halogen lamp and a 40 × objective with integration time of 500 ms. B) Linear relationship between AuNPs counts and thrombin concentrations. The error bar was the standard deviation value of three repetitions.

Table 1
Performance comparison of the thrombin biosensor based on different methods.

Analytical methods	Materials	Linear range	Detection limit	Reference
Colorimetry	aptamer-AuNPs	0.1–15 nM	0.1 nM	[37]
Colorimetry	DNA-hemin- graphene	0–250 nM	0.5 nM	[38]
Fluorescence.	fluorescence aptamer sensor	0–50 nM	2 nM	[39]
Electrochemiluminescence	chromium-loaded CdS nanoprobe	10 fM–100 pM	6.8 fM	[40]
Electrochemistry	three-stranded DNA complexes	5 pM–1 nM	1.7 pM	[41]
Electrochemistry	AuPd nanoparticles	100 fM–20 nM	20 fM	[42]
Photoelectrochemical	C_3N_4/TiO_2 composite	0.0005–5 nM	0.12 pM	[43]
Surface enhancement Raman spectroscopy	two- dimensional nanoarray interface	0.1–10 μM	0.1 μM	[44]
Dark field microscopy	aptamer-AuNPs-MBs	6 fM–100 fM	2.64 fM	This work

field microscope. Therefore, the background light intensity can be reduced, and the effect of reducing background deviation is achieved. It can be seen from Fig. 3A that the number of AuNPs increased markedly with the increase of thrombin addition. Fig. 3B shows that there was a linear correlation between the count values and thrombin concentrations in the range of 6–100 fM with the LOD 2.54 fM, showing that the low concentration of thrombin could be quantitatively detected by the biosensor using this method.

Many methods can be used to detect thrombin, such as colorimetry [37,38], fluorescence [39], electrochemiluminescence [40], electrochemistry [41,42], photoelectrochemical [43] and surface enhancement Raman spectroscopy [44]. Compared to other thrombin detection methods reported previously, our method offers high sensitivity with low LOD (Table 1) by employing DFM imaging process for plasmonic particle enumeration. This ultrasensitive and convenient strategy has overwhelming advantages in detecting low abundance target.

As is well-known, the greatest advantage of biosensors is the specificity to their targets. To assess the specificity of detection, cytochrome, lysozyme, IgG, BSA and trypsin were selected and tested at the concentration of 1 μM, while the tested concentration of thrombin was 100 nM. As is clearly shown in Fig. 4, 100 nM thrombin showed a much stronger response at the absorbance at 530 nm than 1 μM of the other interferences, suggesting that this biosensor has high specificity.

To test the practicality of our biosensor, the detection of thrombin in fetal bovine serum (FBS) was performed. According to the previous report, 60 fM thrombin dissolved in 2% serum [45] was used." [45] was used. The data were shown in Table S1. At the concentration of 60 fM, the recovery were 98% and 104% and the RSD were ranging from 2.12% to 6.36%. The acceptable RSD and good recovery showed this strategy can be applied to detect thrombin in real biological samples.

4. Conclusions

In summary, we developed an ultrasensitive and convenient strategy for the detection of target molecules based on aptamer-target interaction and optical quantification of released AuNPs with single particle sensitivity using a conventional DFM. LOD as low as 2.54 fM has been achieved. The aptasensor with a core-shell structure consisting of MBs, aptamer and AuNPs, was fabricated by complementary hybridization of the DNA probe on the surface of AuNPs to the aptamer coupled to the MBs. Using thrombin as an example, the results of this study demonstrate the general suitability of this core-shell assay for protein detection in buffers and biological media with high sensitivity and specificity and easy operation. Furthermore, the biosensor was sufficiently stable to identify the intended target in the presence of 2% serum which has great potential in the detection of biomarkers in clinical samples. Since there is no special modification on the aptamer, the strategy can be applied not only for different types of aptamers (DNA and RNA) but also for various types of targets (small molecule drugs, and proteins), thus provides a new approach for bioanalysis in general.

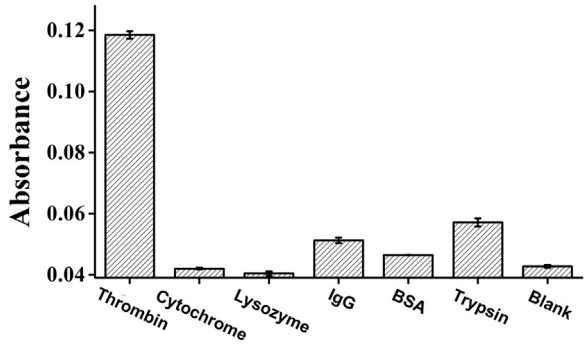

Fig. 4. The specificity of the aptasensor. Thrombin (100 nM), Cytochrome (1 μM), Lysozyme (1 μM), IgG (1 μM), BSA (1 μM), Trypsin (1 μM), and Blank were tested. The error bar is the standard deviation value of three repetitions.

Acknowledgments

This work was supported by the National Science Foundation of China (grants no. 21573124, 21273126) and Fundamental Research Program of Shenzhen (JCYJ20170413104646428, JCYJ20160317152359560, JCYJ20170307153548350 and JCYJ20160324163734374).

Declarations

The authors have no competing interests to declare.

Appendix A. Supporting information

Supplementary data associated with this article can be found in the online version at http://dx.doi.org/10.1016/j.talanta.2018.01.070.

References

[1] J.A. Lindbo, B.W. Falk, The impact of "coat protein-mediated virus resistance" in applied plant pathology and basic research, Phytopathology 107 (6) (2017) 624–634.
[2] D. Abegg, G. Gasparini, D.G. Hoch, A. Shuster, E. Bartolami, S. Matile, et al., Strained cyclic disulfides enable cellular uptake by reacting with the transferrin receptor, J. Am. Chem. Soc. 139 (1) (2016) 231–238.
[3] T. Guo, W. Noble, D.P. Hanger, Roles of tau protein in health and disease, Acta Neuropathol. 133 (2017) 1–40.
[4] D. Lenggenhager, J. Gouttenoire, M. Malehmir, M. Bawohl, H. Honcharova-Biletska, S. Kreutzer, et al., Visualization of hepatitis e virus rna and proteins in the human liver, J. Hepatol. 67 (3) (2017) 471–479.
[5] B. Madhavan, S. Yue, U. Galli, S. Rana, W. Gross, M. Müller, et al., Combined evaluation of a panel of protein and mirna serum-exosome biomarkers for pancreatic cancer diagnosis increases sensitivity and specificity, Int. J. Cancer 136 (11) (2015) 2616–2627.
[6] H. Malekzad, H. Mirshekari, P.S. Zangabad, S.M. Moosavi Basri, F. Baniasadi, A.M. Sharifi, et al., Plant protein-based hydrophobic fine and ultrafine carrier particles in drug delivery systems, Crit. Rev. Environ. Sci. Technol. (2017) 1–21.
[7] D.E. Scott, A.R. Bayly, C. Abell, J. Skidmore, Small molecules, big targets: drug discovery faces the protein-protein interaction challenge, Nat. Rev. Drug. Discov. 15 (8) (2016) 533–550.
[8] G. Arena, E.M. Valente, PINK1 in the limelight: multiple functions of an eclectic

protein in human health and disease, J. Pathol. 241 (2) (2017) 251–263.
[9] T.P. Knowles, M. Vendruscolo, C.M. Dobson, The amyloid state and its association with protein misfolding diseases, Nat. Rev. Mol. Cell. Bio. 15 (6) (2014) 384–396.
[10] M.L. Iaria, S. Fiorentini, E. Focà, S. Zicari, C. Giagulli, F. Caccuri, et al., Synthetic hiv-1 matrix protein p17-based at20-klh therapeutic immunization in hiv-1-infected patients receiving antiretroviral treatment: a phase i safety and immunogenicity study, BMC Inf. Dis. 32 (9) (2014) 1072–1078.
[11] V.L. Elliott, G.T. Edge, M.M. Phelan, L.Y. Lian, R. Webster, R.F. Finn, et al., Evidence for metabolic cleavage of a PEGylated protein in vivo using multiple analytical methodologies, Mol. Pharm. 9 (5) (2012) 1291–1301.
[12] J.W. Lindsey, Antibodies to the Epstein-Barr virus proteins BFRF3 and BRRF2 cross-react with human proteins, J. Neuroimmunol. 310 (2017) 131–134.
[13] I. Saleem, W. Widger, W.K. Chu, A new technique to detect antibody-antigen reaction (biological interactions) on a localized surface plasmon resonance (LSPR) based nano ripple gold chip, Appl. Surf. Sci. 411 (2017) 205–209.
[14] D. Wang, B. Lin, Y. Cao, M. Guo, Y. Yu, A highly selective and sensitive fluorescence detection method of glyphosate based on an immune reaction strategy of carbon dot labeled antibody and antigen magnetic beads, J. Agric. Food Chem. 64 (30) (2016) 6042–6050.
[15] C. Tuerk, L. Gold, Systematic evolution of ligands by exponential enrichment: rna ligands to bacteriophage T4 DNA polymerase, Science 249 (4968) (1990) 505–510.
[16] A.D. Ellington, J.W. Szostak, Selection in vitro of single-stranded DNA molecules that fold into specific ligand-binding structures, Nature 346 (6287) (1990) 818–822.
[17] P. Travascio, Y. Li, D. Sen, Dna-enhanced peroxidase activity of a dna aptamer-hemin complex, Chem. Biol. 5 (9) (1998) 505–517.
[18] D.A. Daniels, H. Chen, B.J. Hicke, K.M. Swiderek, L. Gold, A tenascin-c aptamer identified by tumor cell selex: systematic evolution of ligands by exponential enrichment, Proc. Natl. Acad. Sci. USA 100 (26) (2003) 15416–15421.
[19] M. Darmostuk, S. Rimpelova, H. Gbelcova, T. Ruml, Current approaches in SELEX: an update to aptamer selection technology, Biotechnol. Adv. 33 (2015) 1141–1161.
[20] R.F. Macaya, P. Schultze, F.W. Smith, Thrombin-binding DNA aptamer forms a unimolecular quadruplex structure in solution, Proc. Natl. Acad. Sci. USA 90 (8) (1993) 3745–3749.
[21] P. Fan, A.K. Suri, R. Fiala, Molecular recognition in the FMN-RNA aptamer complex, J. Mol. Biol. 258 (3) (1996) 480–500.
[22] J.R. Lorsch, J.W. Szostak, In vitro selection of RNA aptamers specific for cyanocobalamin, Biochem 33 (4) (1994) 973–982.
[23] J.H. Yeom, M. Joo, B. Lee, K.P. Kim, N.C. Ha, Y. Park, et al., Intracellular delivery of recombinant proteins via gold nanoparticle–dna aptamer composites is independent of the protein physicochemical properties and cell type, J. Ind. Eng. Chem. 45 (2017) 5–10.
[24] T. Wagner, H.G. Lipinski, M. Wiemann, Dark field nanoparticle tracking analysis for size characterization of plasmonic and non-plasmonic particles, J. Nanopart. Res. 16 (5) (2014) 2419.
[25] Y. Zhao, L. Gui, Z. Chen, Colorimetric detection of Hg2+ based on target-mediated growth of gold nanoparticles, Sens. Actuators B-Chem. 241 (2017) 262–267.
[26] N. Kumar, R. Seth, H. Kumar, Colorimetric detection of melamine in milk by citrate-stabilized gold nanoparticles, Anal. Biochem. 456 (1) (2014) 43–49.
[27] J. Shi, C. Chan, Y. Pang, W. Ye, F. Tian, J. Lyu, et al., A fluorescence resonance energy transfer (FRET) biosensor based on graphene quantum dots (GQDs) and gold nanoparticles (AuNPs) for the detection of mecA gene sequence of Staphylococcus aureus, Biosens. Bioelectron. 67 (2015) 595–600.
[28] L. Tan, Z. Chen, Y. Zhao, X. Wei, Y. Li, C. Zhang, et al., Dual channel sensor for detection and discrimination of heavy metal ions based on colorimetric and fluorescence response of the AuNPs-DNA conjugates, Biosens. Bioelectron. 85 (2016) 414–421.
[29] Z. Xi, R. Huang, Y. Deng, E. Su, N. He, The chemiluminescence aptasensor based on magnetic separation and double-functionalized AuNPs for the detection of human thrombin, Sci. Adv. Mater. 8 (2016) 1678–1682.
[30] J. Zhao, Y. Zhang, H. Li, Y. Wen, X. Fan, A non-enzymatic glucose sensor based on the composite of cubic Cu nanoparticles and arc-synthesized multi-walled carbon nanotubes, Biosens. Bioelectron. 26 (5) (2011) 2297–2303.
[31] (a) Y. Lai, S. Sun, T. He, S. Schlucker, et al., Raman-encoded microbeads for spectral multiplexing with SERS detection, RSC Adv. 5 (18) (2015) 13762–13767; (b) S. Sun, D. Thompson, U. Schmidt, et al., Micro/nano-patterning of DNA and rapid readout with SERS tags, Chem. Comm. 46 (29) (2010) 5292–5294; (c) Z. Mu, X. Zhao, Z. Xie, Y. Zhao, Q. Zhong, L. Bo, et al., In situ synthesis of gold nanoparticles (aunps) in butterfly wings for surface enhanced raman spectroscopy (sers), J. Mater. Chem. B.B 1 (11) (2013) 1607–1613.
[32] G. Li, L. Zhu, Z. Wu, Y. He, H. Tan, S. Sun, Digital concentration readout of dna by absolute quantification of optically countable gold nanorods, Anal. Chem. 88 (22) (2016) 10994–11000.
[33] T. Li, X. Xu, G. Zhang, R. Lin, Y. Chen, C. Li, et al., Nonamplification sandwich assay platform for sensitive nucleic acid detection based on aunps enumeration with the dark-field microscope, Anal. Chem. 88 (8) (2016) 4188–4191.
[34] H. Yang, J. Ji, Y. Liu, J. Kong, B. Liu, An aptamer-based biosensor for sensitive thrombin detection, Electrochem. Commun. 11 (2009) 38–40.
[35] Y. Peng, L. Li, X. Mu, L. Guo, Aptamer-gold nanoparticle-based colorimetric assay for the sensitive detection of thrombin, Sens. Actuators B. 177 (2013) 818–825.
[36] X. Cheng, D. Dai, Z. Yuan, L. Peng, Y. He, E.S. Yeung, Color difference amplification between gold nanoparticles in colorimetric analysis with actively controlled multiband illumination, Analyt. Chem 86 (15) (2014) 7584–7592.
[37] Z. Chen, L. Tan, L. Hu, Y. Zhang, S. Wang, F. Lv, Real colorimetric thrombin aptasensor by masking surfaces of catalytically active gold nanoparticles, ACS Appl. Mater. Interfaces 8 (1) (2016) 102–108.
[38] B. Lin, Q. Sun, K. Liu, D.Q. Lu, Y. Fu, Z.A. Xu, W. Zhang, Label-free colorimetric protein assay and logic gates design based on the self-assembly of hemin-graphene hybrid nanosheet, Langmuir 30 (2014) 2144–2151.
[39] X. Liu, L. Shi, X. Hua, Y. Huang, S. Su, Q.L. Fan, L.H. Wang, W. Huang, Target-induced conjunction of split aptamer fragments and assembly with a water-soluble conjugated polymer for improved protein detection, ACS Appl. Mater. Interfaces 6 (2014) 3406–3412.
[40] Q.Q. Wen, P. Lu, P.H. Yang, A glassy carbon electrode modified with in-situ generated chromium-loaded CdS nanoprobes and hep- arin for ultrasensitive electrochemiluminescent determination of thrombin, Microchim. Acta 183 (1) (2016) 123–132.
[41] J. Yang, B. Dou, R. Yuan, Y. Xiang, Aptamer/protein proximity binding-triggered molecular machine for amplified electrochemical sensing of thrombin, Anal. Chem. 89 (9) (2017) 5138–5143.
[42] X. Wang, D. Sun, Y. Tong, Y.S. Zhong, Z.G. Chen, A voltammetric aptamer-based thrombin biosensor exploiting signal amplification via synergetic catalysis by DNAzyme and enzyme decorated AuPd nanoparticles on a poly(o-phenylenediamine) support, Microchim. Acta 184 (6) (2017) 1–9.
[43] D.W. Fan, C.J. Guo, H.M. Ma, D. Zhao, Y.N. Li, D. Wu, Q. Wei, Facile fabrication of an aptasensor for thrombin based on graphitic carbon nitride/TiO2 with high visible-light photoelectrochemical activity, Biosens. Bioelectron. 75 (2016) 116–122.
[44] Y. Deng, X. Yue, H. Hu, X.D. Zhou, A new analytical experimental setup combining quartz crystal microbalance with surface enhancement Raman spectroscopy and its application in determination of thrombin, Microchem. J. 385 (6) (2017).
[45] K.C. Lin, B. Jagannath, S. Muthukumar, S. Prasad, Sub-picomolar label-free detection of thrombin using electrochemical impedance spectroscopy of aptamer-functionalized MoS2, Analyst 142 (15) (2017) 2770–2780.